Distribution of the order parameter of the coil-globule transition

J. B. Imbert, A. Lesne, and J. M. Victor
Laboratoire de Physique Théorique des Liquides, Université Pierre et Marie Curie, Case courrier 121, 4 Place Jussieu, 75252 Paris Cedex 05, France

(Received 7 October 1996; revised manuscript received 18 June 1997)

We investigate the probability distribution $\mathcal{P}_N(r)$ of the radius of gyration r of a polymer chain of size N with excluded-volume interactions at infinite temperature. This function shows the geometric contribution to the tricritical coil-globule transition of self-avoiding walks; it indicates that the relevant order parameter t of the transition is a power of the density $\rho = Nr^{-d}$. The theoretical form of the distribution $P_N(t)$ of this order parameter is deduced from scaling arguments, and supported by numerical simulations. Intending to probe the contribution of the different subsets of conformations, namely, globule, coil and stretch, we supplement $P_N(t)$ with a formal Boltzmann factor; this model undergoes a tricritical coil-globule transition which is solved exactly. We show a nontrivial finite-size scaling for $P_N(t)$ and analyze its convergence toward the thermodynamic limit. Due to the presence in $P_N(t)$ of a diverging factor t^c with $c<-1$, this convergence happens to be tragically slow. As a result, the scaling behavior observed in numerical simulations is qualitatively different from its thermodynamic limit, and we relate the critical exponents of the geometric transition in the thermodynamic limit and the effective exponents observed at finite size. [S1063-651X(97)12010-4]

PACS number(s): 36.20.Ey, 64.60.Kw, 75.40.Mg

I. INTRODUCTION

Since the pioneering work of de Gennes [1], much of the literature has been devoted to the status of the coil-globule transition. Even though its tricritical nature soon became commonly accepted, achieving a complete scaling theory motivated many controversial papers [2] and is still an open problem. All the exponents were theoretically calculated in two dimensions for one specific model [3], but it has not been possible to solve more realistic cases, even the simplest ones.

The present paper raises the following question: which properties of the coil-globule transition come from the geometric structure of the chain (i.e., the linear ordering of the monomers along the chain and the excluded-volume effects) and which ones come from specific interactions between monomers (typically van der Waals and Coulomb)? We bring about some answers by studying the statistics of the radius of gyration, using a phenomenological approach supported by a numerical simulation. This analysis indeed provides universal insights about the different classes of conformations (namely globule, coil, and stretch) and on the transitions between them.

Restricting to a lattice description, geometric properties are mimicked using the well-known self-avoiding walk model (hereafter denoted the SAW model, as usual). It is worth noticing that the simple SAW description coincides with the infinite temperature limit of any realistic model including interactions between monomers and solvent. In that sense, geometric properties are universal insofar as they lay behind any realistic model but do not depend on the associated interactions. The relevant order parameter for describing the coil-globule transition is generally taken to be $\psi = \sqrt{NR_G^{-d}}$, where R_G is the usual radius of gyration defined as the root-mean-square over all the conformations of the *random* quantity $r = N^{-1}\sqrt{\Sigma_{1\leqslant i<j\leqslant N}||\mathbf{r}_i - \mathbf{r}_j||^2}$ for a chain of N monomers. In order to obtain more statistical information about the conformations, here we investigate the distribution of the random variable $\psi = \sqrt{Nr^{-d}}$; the usual quantity ψ is nothing but the first moment of this distribution. The simple relation between the random variables ψ and r allows us to focus on $\mathcal{P}_N(r)$ without losing any information. Here $\mathcal{P}_N(r)dr$ denotes the probability that a SAW of size N has a radius of gyration between r and $r+dr$; it completely describes the geometric properties of SAWs and is universal for linear polymers.

Victor and Lhuillier [4] already investigated the form of $\mathcal{P}_N(r)$ in the domain where the radius of gyration scales as $r \sim N^{\nu}$ (ν being the usual Flory exponent). They proposed a scaling law for $\mathcal{P}_N(r)$ in two dimensions which agrees with their numerical simulation data. This work was soon reproduced in three dimensions by Bishop and Saltiel [5], but still in this rather narrow interval of values of r. Please note that we henceforth denote $\sim$ the identity of the leading orders up to some multiplicative constants where, unless explicitly mentioned, the asymptotic ordering is associated with the limit $N \to \infty$.

The radius of gyration describes the nature of the conformations of the chain. It increases from its minimum value $r_{\min} = \zeta_{\min} N^{1/d}$ to its maximum value $r_{\max} = \zeta_{\max} N$ (see Table I for the value of $\zeta_{\min}$ in three dimensions). The conformations are commonly divided into three classes, namely globule, coil, and stretch, according to their own radius of gyration r:

globule	coil	stretch
$r \sim N^{1/d}$	$r \sim N^{\nu}$	$r \sim N$

Because the polymer changes continuously from a globule into a coil and from a coil into a stretch, the limits between these classes are rather fuzzy. More precisely, a clear-cut distinction between the three regimes is relevant *only* in the thermodynamic limit ($N \to \infty$) but clearly *not* at finite size N. We suggest that the distribution $\mathcal{P}_N(r)$ allows one to define

TABLE I. Numerical values of the connectivity constants μ and ω of a self-avoiding walk on a cubic lattice for coil and compact globular conformations, respectively. $t_{\max}$ denotes the maximum value of t, and $g(t_{\max})$ is given in Fig. 1. The value of μ comes from exact enumeration [8] and $\omega=(2d/e)$ according to Ref. [21]. Here we used the slithering snake algorithm as it involves the same lattice model (a monomer occupies one site and the length bond is equal to 1).

$\zeta_{\min}$	$t_{\max}$	$g(t_{\max})$	μ	ω	$\ln(\mu/\omega)$
0.4805	15.63	0.770 ± 0.015	4.683	2.21	0.751

three phases and associated transitions. The issue is then to properly carry out the thermodynamic limit of the distribution in order to bring out the phase transitions and characterize their nature in the usual thermodynamic sense.

In Sec. II, we recall scaling arguments which indicate the relevant form of $\mathcal{P}_N(r)$ and lead us to introduce a new variable t; we believe its first moment $\langle t\rangle$ to be the most suitable order parameter for the coil-globule transition. In Sec. III, we give the complete theoretical structure of the distribution $P_N(t)$ of the state variable t. Section IV is devoted to a numerical justification of the structure of $P_N(t)$, and to the measure of a new geometric exponent n appearing in it; moreover, we show a novel factor t^c contributing to $P_N(t)$. In Sec. V, we prove by introducing a fictitious (however strongly related with more realistic models) Boltzmann factor that the structure of $P_N(t)$ induces an intrinsic coil-globule transition which we claim to be the geometric foundation of real coil-globule transitions. In Sec. VI, we examine the scaling properties of $P_N(t)$ and of its moments; we also compute their thermodynamic limit. In Sec. VII we deduce the critical exponents ν_θ and ϕ for this transition; we discuss the nature of the transition according to the position of the exponent c with respect to a threshold value $c^*=-1$. The observed value $c<-1$ leads to an anomalous tricritical scaling behavior. Section VIII is devoted to finite-size problems. Due to the value $c<-1$, it is shown that the thermodynamic limit is reached so slowly that it cannot be described by numerical data and cannot predict observable results (except for unrealistic chain lengths of $N\sim10^{20}$ monomers). These data bring out an effective scaling behavior characterized by two different values of the exponent ν_θ, in contrast to the thermodynamic scaling behavior. The previous discussion provides the framework for a correct and exhaustive analysis of our numerical data, which is presented in Sec. IX.

II. SCALING HYPOTHESIS IN THE THREE PHASES

The scaling laws for the distribution $\mathcal{P}_N(r)$ have already been introduced in preceding papers [6] on the basis of phenomenological arguments; here we give further justifications based on the differing statistical scale invariances inside each of the three classes of conformations, which in addition physically comfort their different status.

(a) The globule phase is dominated by *spatially homogeneous* conformations. This means that the local averaged density does not depend on the position inside a given globule and hence coincides with its global density $\rho=Nr^{-d}$. As a result, the probability $\mathcal{P}_N(r)$ scales (up to some normalization constants) as

$$\text{globule}\quad \mathcal{P}_N(r)dr\sim[p(Nr^{-d})]^N d(Nr^{-d})=[p(\rho)]^N d\rho. \tag{1}$$

This assertion involves only the leading behavior of the N dependence of $\mathcal{P}_N(r)$ in the thermodynamic limit $N\to\infty$, as will be discussed below.

(b) In the stretch phase, the length parameter $l=d_{ij}/|j-i|$ is defined as the ratio of the distance d_{ij} between two monomers i and j to their distance $|j-i|$ along the chain; the relevant scale invariance here is the *translational invariance* along the chain. As a result, the parameter l is constant, and hence equal to $l=r_{1N}/N$, where r_{1N} is the so-called end-to-end distance. The same reasoning is still valid when replacing the partial distance d_{ij} by the partial radius of gyration r_{ij}. This invariance is supplemented by the fact that, due to the absence of excluded-volume effects between subsections of the stretch, the chain can here be considered as a succession of *independent parts*, which leads to the following scaling behavior:

$$\text{stretch}\quad \mathcal{P}_N(r)dr\sim[q(r/N)]^N d(r/N). \tag{2}$$

(c) Conversely, the coil phase is dominated by *fractal* conformations (in a statistically defined meaning) of fractal dimension $1/\nu$. Hence $\mathcal{P}_N(r)$ exhibits the following scaling behavior:

$$\text{coil}\quad \mathcal{P}_N(r)dr\sim\Pi(rN^{-\nu})d(rN^{-\nu}). \tag{3}$$

Because the three kinds of behavior (globule, stretch and coil) appear as three limiting cases of a *unique* underlying distribution, some strong matching conditions first introduced in Ref. [6] must be satisfied. Let us recall them briefly. Writing the distribution $p(\rho)$ as

$$p(\rho)=e^{-G(\rho)}, \tag{4}$$

and the distribution $\Pi(rN^{-\nu})$ as

$$\Pi(rN^{-\nu})=e^{-f(rN^{-\nu})}, \tag{5}$$

and assuming that the function G is a power law $G(\rho)\sim\rho^\alpha$ at vanishing density, Eqs. (1), (3), (4) and (5) lead to

$$e^{-NG(Nr^{-d})}\sim e^{-f(rN^{-\nu})} \tag{6}$$

(still identifying the leading order of the N dependences). This leads to

$$f(rN^{-\nu})\sim N(Nr^{-d})^\alpha\sim(rN^{-\nu})^{-d\alpha}, \tag{7}$$

from which it follows that

$$\alpha=\frac{1}{\nu d-1}. \tag{8}$$

Hence, we may rewrite Eqs. (1) and (3) as follows:

$$\text{globule}\quad p\left(\frac{N}{r^d}\right)\sim e^{-A(N/r^d)^{1/(\nu d-1)}}, \tag{9}$$

$$\text{coil} \quad \Pi\left(\frac{r}{N^{\nu}}\right) \sim e^{-A(r/N^{\nu})^{-1/(\nu-1/d)}}, \tag{10}$$

where A is a model-dependent constant. The new state variable

$$t = \rho^{1/(\nu d-1)} \tag{11}$$

arises in a natural way, and we finally come to

$$\text{globule} \quad p\left(\frac{N}{r^{d}}\right) \sim e^{-At}, \tag{12}$$

$$\text{coil} \quad \Pi\left(\frac{r}{N^{\nu}}\right) \sim e^{-NAt}. \tag{13}$$

Such a procedure may be carried out between the coil and the stretch behaviors as well leading to

$$\text{coil} \quad \Pi\left(\frac{r}{N^{\nu}}\right) \sim e^{-A'(r/N^{\nu})^{\delta}}, \tag{14}$$

$$\text{stretch} \quad q\left(\frac{r}{N}\right) \sim e^{-A'(r/N)^{\delta}} \tag{15}$$

for a value $\delta = 1/(1-\nu)$ which is nothing but the Fisher exponent [7]. Now in order to obtain a compact form which embeds the three behaviors and is suitable for the numerical analysis, a simple interpolation is used: defining $P_N(t)$ through the relationship

$$\mathcal{P}_N(r)dr = -P_N(t)dt \tag{16}$$

(let us recall that t is a decreasing function of r), the interpolation writes

$$P_N(t) \sim e^{-[ANt + A'(Nt)^{-q}]}, \tag{17}$$

where

$$q = \frac{\nu - 1/d}{1-\nu}. \tag{18}$$

Let us note that the distribution $P_N(r_{1N})$ of the end-to-end distance r_{1N}, although more often encountered in the literature, is not suited for our purpose for the reason that this distance r_{1N} does not characterize the conformations of the chains. For example, loops, which correspond to $r_{1N}=1$ (on a lattice), may belong to coil as well as to globule classes. A misunderstanding may come from the fact that the *average* value $\langle r_{1N} \rangle$ over subsets of conformations corresponding *respectively*, to globule, coil, or stretch type happens to satisfy the scaling laws $\langle r_{1N} \rangle \sim N^{1/d}$, $\langle r_{1N} \rangle \sim N^{\nu}$, and $\langle r_{1N} \rangle \sim N$, respectively. Nevertheless, the underlying distribution $P_N(r_{1N})$ does not provide any classification of the conformations. On the contrary, as we focus mainly on the coil-globule transition which is characterized on the very behavior of the density, the radius of gyration r (for each conformation) is the relevant state variable in our problem. Please note that from now on r will denote the radius of gyration of a given conformation (*random variable*) and must not be confused with the usual mean radius of gyration R_G (the *average* over all the conformations). In view of Eq. (17), we shall rather use the state variable t given in Eq. (11).

III. COMPLETE STRUCTURE OF THE DISTRIBUTION $P_N(t)$

Equation (17) arose from matching conditions between scaling arguments based on the homogeneous nature of the globule and stretch conformations on one hand, and on the fractal nature of the coil conformations on the other hand. In order to highlight all the relevant contributions involved in the thermodynamic behavior, we now design a theoretical expression for $P_N(t)$ which remains valid outside the matching domain and thus generalizes Eq. (6). The extra contributions with respect to Eq. (17) will contain the exponents of the geometric transition claimed above and give access to the scaling landscape of the whole space of conformations.

It is well known [8] that the total number $\aleph_N$ of SAW's of length N is given by

$$\aleph_N = \Lambda \mu^N N^{\gamma-1}, \tag{19}$$

where μ is the connectivity constant of the lattice, γ is the so-called enhancement exponent, and Λ is a lattice-dependent constant. We now focus on the globule domain corresponding to values $t = O(1)$. It has become well accepted that the number $\aleph(t,\Delta t)$ of globule conformations of a given density (corresponding to values between t and $t+\Delta t$) similarly behaves according to

$$\aleph(t,\Delta t) = \Lambda(t,\Delta t)\mu(t)^N N^{\gamma_g - 1}. \tag{20}$$

Here, Δt is a narrow interval which is fixed *independently of* N. The number $\mu(t)$ is the connectivity constant of SAW's with a density $\rho = t^{\nu d-1}$, and $\Lambda(t,\Delta t)$ is a prefactor still to be modeled. The exponent γ_g does not vary with t (in the whole globule domain), and characterizes the globule in the same way as γ does for the coil. Equation (20) is to be compared with the partition function of an interacting self-avoiding walk given in Ref. [9], although we do not include their term $[\mu_1(\rho)]^{N^{\sigma}}$ (with $\sigma = 1-1/d$). We have shown indeed in a preceding paper [10] that this term arises from the energetic contribution of the nearest-neighbor interactions (see also Sec. V). By definition, $\aleph(t,\Delta t) = \aleph_N P_N(t)\Delta t$, which leads to

$$P_N(t) = \frac{\Lambda(t,\Delta t)}{\Lambda \Delta t}\left[\frac{\mu(t)}{\mu}\right]^N N^{\gamma_g - \gamma}, \tag{21}$$

where $\Lambda(t,\Delta t)[\Lambda \Delta t]^{-1}$ does not depend on Δt. This proves that the leading N dependence of $P_N(t)$ is expressed as

$$P_N(t) \sim e^{-Ng(t)}, \tag{22}$$

where a mere identification gives

$$e^{-g(t)} = \frac{\mu(t)}{\mu}. \tag{23}$$

Conjecturing a power law for $\Lambda(t,\Delta t)[\Lambda \Delta t]^{-1}$, we come to the complete expression

$$P_N(t) = \lambda N^{\gamma_g - \gamma} t^{c} e^{-Ng(t)}, \tag{24}$$

TABLE II. Theoretical values (for $d=2$) or numerical measurements (for $d=3$) of the des Cloizeaux exponents θ_0 and of the enhancement exponents γ in the coil and in the globule phases. The last column displays the value of c as deduced from Eq. (27). In three dimensions, the value of c is still unknown but the interval is rather narrow (5%).

	θ_0	θ_0^g	γ	γ_g	c
$d=2$	$\frac{11}{24}$	$\frac{3}{8}$	$\frac{43}{32}$	$\frac{19}{16}$	$-\frac{37}{32}$
$d=3$	27	<0.27	1.1608	-1.09	$-1.16\leqslant c\leqslant -1.07$

where λ is a normalization constant *independent of* N; this independence will be used for testing the internal consistency of our scaling theory (Secs. IV and IX). Let us finally compute the exponent c. Keeping in mind that the distribution $P_N(t)$ is related to the distribution $\mathcal{P}_N(r)$ through Eq. (16), and that, according to the very definition of t [Eq. (11)] we have $dr/dt=(1/d-\nu)N^{\nu+1}(Nt)^{-1-(\nu-1/d)}$, we obtain

$$P_N(t=1/N)=(\nu-1/d)N^{1+\nu}\mathcal{P}_N(r=N^\nu). \tag{25}$$

It has already been shown in Ref. [4] that $N^\nu\mathcal{P}_N(r=N^\nu)$ is independent of N, so that

$$P_N(t=1/N)\sim N. \tag{26}$$

Comparing with Eq. (24), we finally come to the explicit relation

$$c+1=\gamma_g-\gamma. \tag{27}$$

This relation asserts the universality of c, which provides another test of consistency of our scaling predictions. Let us note that this exponent c is equivalent for the distribution $P_N(t)$ to the des Cloizeaux exponent θ_0 involved in the distribution of the end-to-end distance [11]. It is well known that γ and θ_0 are related through $\theta_0=(\gamma-1)/\nu$. Duplantier similarly introduced an exponent θ_0^g in the globule domain, and gave its exact value $\theta_0^g=\frac{3}{8}$ in two dimensions [12]; γ_g is related to θ_0^g through

$$\gamma_g=1+\frac{\theta_0^g}{d}. \tag{28}$$

This leads to $\gamma_g=\frac{19}{16}$ in the globule domain, whereas in the coil domain [13] $\gamma=\frac{43}{32}$. In three dimensions, the des Cloizeaux exponents θ_0 and θ_0^g are not known exactly but numerical simulations [14] lead to $\theta_0=0.27\pm0.01$. Another related result [15] is $\gamma=1.1608\pm0.0003$. From Eq. (27) we deduce $c=-\frac{37}{32}$ in two dimensions. We conjecture that the physical reasons explaining in two dimensions why $0<\theta_0^g<\theta_0$ remain valid in three dimensions, so that $-\gamma<c<-\gamma-\theta_0/3$; hence $-1.16\leqslant c\leqslant -1.07$ in three dimensions (see Table II for a summary of the discussion). The forthcoming analysis of the geometric coil-globule transition gives an improved value $c=-1.13\pm0.01$; hence $\gamma_g=1.03\pm0.01$ and finally $\theta_0^g=0.09\pm0.03$ according to Eq. (28).

TABLE III. Details of the Monte Carlo simulations (slithering snake algorithm). For each size N, between two and four histograms (corresponding to different values of κ) were computed and collapsed in a global histogram spanning the overall interval of t values. Column 2 gives the sum of the number of steps (one simulation step corresponding to the move of one monomer) required for each histogram. For each pair (N,κ), the number of independent conformations is the ratio of the total number of simulation steps to the so-called decorrelation time. Column 3 gives the overall number of independent conformations obtained for a given N and all the corresponding values of κ.

N	No. of steps ($\times10^6$)	No. of Ind. Conf.
20	25	200 735
50	710	205 777
80	710	73 065
100	1220	47 617
150	3210	106 485

We extend the validity of the expression $P_N(t)=\lambda N^{1+c}t^c e^{-Ng(t)}$ [Eq. (24)] to the coil state by including the factor $e^{-A'(Nt)^{-q}}$ already encountered in Eq. (17), to obtain the complete expression

$$P_N(t)=\lambda N^{1+c}t^c e^{-Ng(t)}e^{-A'(Nt)^{-q}}, \tag{29}$$

where q is given in Eq. (18) and t is defined in Eq. (11).

IV. NUMERICAL EVIDENCE OF THE STRUCTURE OF $P_N(t)$

In order to check the theoretical description of $P_N(t)$ and further model the function $g(t)$, we performed a numerical simulation. We first used the ''slithering snake'' (SS) algorithm of Wall and Mandel [16] on a cubic lattice for chain lengths N between 20 and 150 monomers (see Table III for details). This is associated with a discrete modeling of the chain in which each monomer occupies a site of the lattice and the bond length is fixed, being equal to the lattice parameter. In order to lower lattice effects and to bypass the nonergodicity of the SS algorithm, we also used the ''bond fluctuation'' (BF) algorithm of Carmesin and Kremer [17]. This appears as a nearly off-lattice model as the bond length varies from $l_{\min}=2$ to a value $l_{\max}$ equal to $\sqrt{13}$ in $d=2$ and $\sqrt{10}$ in $d=3$. Before discussing with more details the statistical validity and the physical relevance of these two approaches, let us present the common procedure used to generate the numerical data and the subsequent analysis.

In both approaches, the excluded volume has been taken into account by imposing that two distinct monomers never occupy the same cell, which amounts to imposing a minimal distance $l_{\min}=1$ for the SS algorithm and $l_{\min}=2$ for the BF algorithm between any pair of monomers. The range of values of the radius of gyration reached in the former simulations presented in Refs. [4] and [5] was rather narrow and did not provide compact conformations. In order to enlarge this interval and to sample values of r around the minimum value $r_{\min}=\zeta_{\min}N^{1/d}$, it was necessary to use a bias of selection in our Monte Carlo simulation (such a bias is usually called

TABLE IV. Dimensionless coefficients entering the probability distribution of the radius of gyration in three dimensions, obtained by the numerical analysis (Sec. IX) of the data coming from the slithering snake (SS) algorithm and bond fluctuation (BF).

	n	c	A	B	A'	λ
SS	2.1 ± 0.1	-1.13 ± 0.01	0.0215 ± 0.0005	$(8.3\pm0.2)\times10^{-4}$	15.0 ± 1	1.95 ± 0.05
BF	2.1 ± 0.1	-1.13 ± 0.01	0.025 ± 0.001	$(4.1\pm0.2)\times10^{-4}$	1.5 ± 0.2	$(2.0\pm0.1)\times10^{-4}$

''importance sampling''). Instead of the usual Boltzmann weight, we introduced in the Metropolis procedure an effective Boltzmann factor of the form $e^{\kappa Nt}$, where κ is an adjustable parameter playing the role of an effective inverse temperature. Because of the lattice, the variable t is discrete. However, the interval δt between two consecutive discrete values is very small, so that we divided the interval of t values into subintervals of arbitrary fixed length $\Delta t=0.05$ (for which $\Delta t \gg \delta t$). The numerical value $P_N(t)\Delta t$ accounts for the fraction of conformations that have a t value between t and $t+\Delta t$. Note that in order to take into account the variable bond length in the BF method, we used a rescaled density

$$\rho^* = N\left(\frac{\langle l\rangle(\rho)}{r}\right)^d \Leftrightarrow t^* = t[\langle l\rangle(t)]^{d/(\nu d-1)}. \tag{30}$$

Here $\langle l\rangle(t)$ (or equivalently $\langle l\rangle(\rho)$ as t and ρ are related) is the average bond length for a given value of t (the average being taken over the N bonds of the chain and over all the conformations corresponding to the t value).

It is sufficient to run the simulation for a few values of κ to cover the entire space of conformations. It is then necessary to collapse the data obtained at different values of κ into a single histogram. We did so in a manner which, although reminiscent of that of Ferrenberg and Swendsen [18], is, however, substantially different and is completely described in Ref. [19].

In order to check the validity of Equation (29), we draw the ratio $-(1/N)\ln[\lambda^{-1}N^{-(1+c)}t^{-c}P_N(t)e^{A'(Nt)^{-q}}]$ as a function of t for different chain lengths. Note that the numerical value of A' was yet known for the SS algorithm from the direct graphical analysis of $\mathcal{P}_N(r)$ [5]. For a unique suitable fit of λ and c (see Table IV), the curves collapse onto a universal curve $g(t)$ (see Figs. 1 and 2). The fit is very sensitive to the value of c. It allows one to give an accurate estimate $c=-1.13\pm0.01$, and shows in particular its position as regards -1. The universality strongly supports the scaling theory for $P_N(t)$ presented in Sec. III.

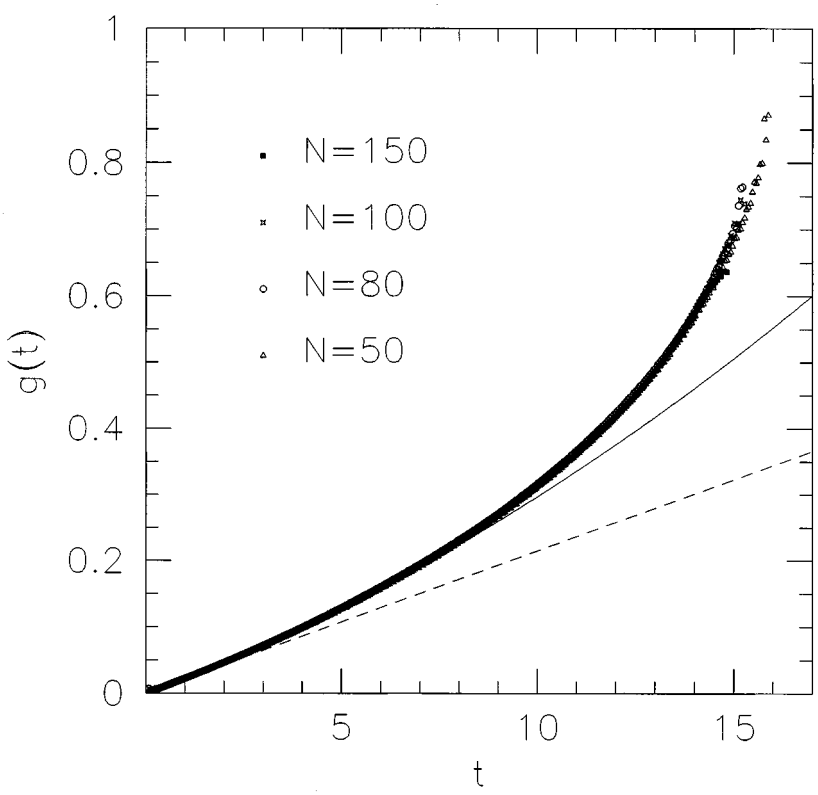

FIG. 1. Log-log plot of the universal function $g(t)$ as a function of t. The curves obtained from the slithering snake algorithm and for different chain lengths collapse onto a single one. For small values of t, $g(t)$ is linear with a slope $A=0.0215\pm0.0005$. The dashed line accounts for this linear behavior, whereas the plain line displays the second-order approximation given in Eq. (31). Compare with Fig. 2, obtained with the bond-fluctuation algorithm.

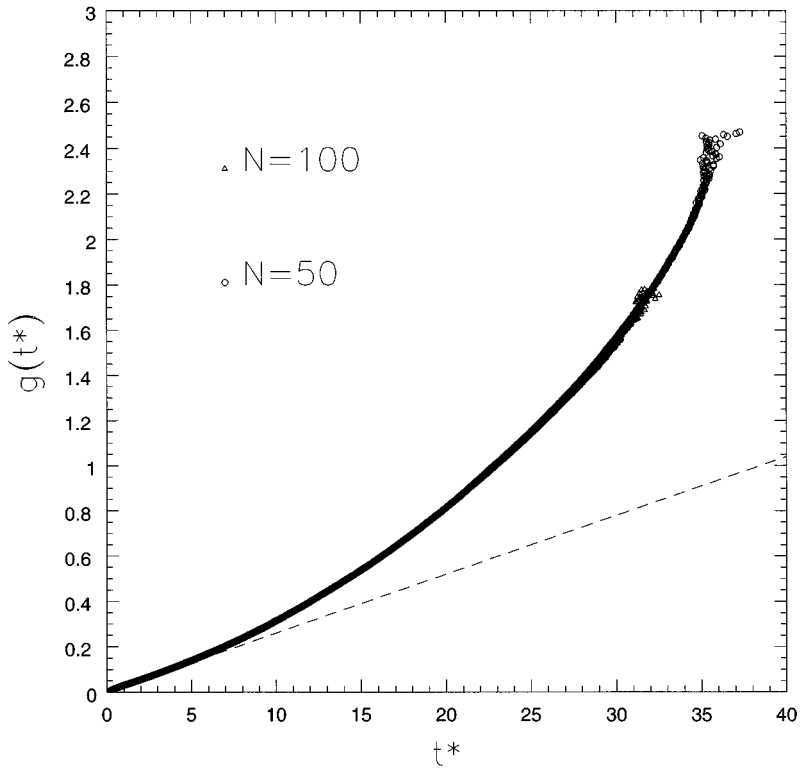

FIG. 2. Log-log plot of the universal function $g(t^*)$ as a function of t^* for the bond-fluctuation algorithm. t^* is defined in Eq. (30). For small values of t^*, $g(t^*)$ is linear with a slope $A=0.025\pm0.001$. Compare with Fig. (1) obtained with the slithering snake algorithm.

Let us briefly discuss the respective pitfalls and advantages of the SS and BF simulations. A major drawback of the SS algorithm is its nonergodicity. Nevertheless, the large amount of available results (for example from exact enumeration) about the statistics of SAW's on square and cubic lattices comparing favourably with SS numerical results weakens this criticism. Moreover, we are mainly interested in the behavior at vanishing t, which corresponds to low-density conformations; as the nonergodicity of the SS algorithm comes from certain dense conformations [20], it is likely that the sampling of the coil conformations is not flawed. Concerning the sampling of the dense region, we are inclined to think that the nonergodicity uniformly restricts the sampling, so that the overall statistics is unbiased. Indeed, let us define ω as the limiting value of the connectivity constant $\mu(t)$ for close-packed SAW's corresponding to the subset $t=t_{\max}$ of the globule regime. Our function $g(t)$ involves this coefficient ω through $g(t_{\max})=\ln(\mu/\omega)$ [see Eq. (23) and Table I], and the good agreement between our value of ω and the value computed in Ref. [21] supports the relevance of our SS simulation even in the dense region.

As the BF algorithm is ergodic, the compatibility of the results obtained with BF and SS simulations about the scaling form of $P_N(t)$ comforts the claim that the statistics obtained by the SS algorithm at vanishing t is unaffected by its nonergodicity. The values of the exponent c extracted from SS and BF data coincide (Figs. 1 and 2). As the *models* underlying the two simulation differ, this agreement strongly supports the universal scaling form of $P_N(t)$ proposed in Eq. (29); in particular, it does not depend on the discrete nature of the modeling, and hence should actually stand for real chains in the continuum.

Further modeling of $g(t)$ is the purpose of the following sections. According to Figs. 1 and 2, $g(t)$ is linear for small values of t, in agreement with the theoretical predictions. A direct analysis presented in Figs. 3 (for the slithering snake simulation) and 4 (for the bond fluctuation simulation) shows that the first correction to this linear behavior is a power law:

$$g(t)=At+Bt^n+\text{h.o.}, \tag{31}$$

where h.o. represents higher order terms. Nevertheless, the procedure is not able to provide a more accurate value for n than $n=2\pm0.2$ for the SS simulation and $n=2.2\pm0.2$ for the BF simulation. As the two confidence intervals overlap, we claim that both simulations are consistent with the universal scaling form given in Eqs. (29) and (31), with $n=2.1\pm0.1$. The more refined numerical analysis presented below for the slithering snake simulation (Sec. IX) will comfort this value.

V. GEOMETRIC COIL-GLOBULE TRANSITION. GEOMETRIC Θ POINT

Let us consider a model of fictitious interactions between monomers leading to the following energy of the whole chain,

$$U=-NJt. \tag{32}$$

J is a coupling parameter. Note that such interactions are not pairwise additive. This involves a Boltzmann weight

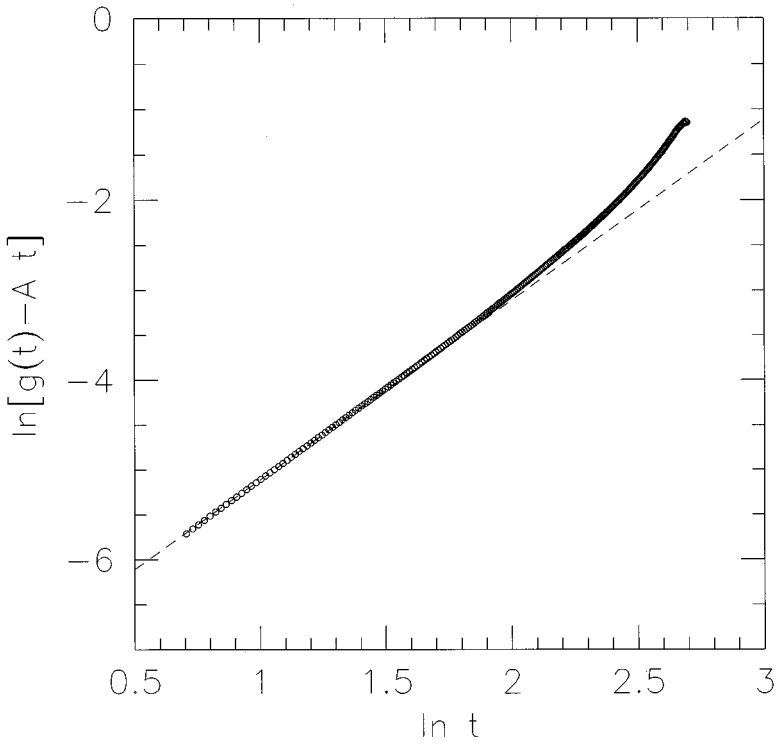

FIG. 3. Log-log plot of the difference $g(t)-At$ as a function of t for the slithering snake algorithm. The slope of the curve is equal to n, and hence shows that the first correction to the linear behavior of $g(t)$ is of the form Bt^n with $B=(8.3\pm0.1)\times10^{-4}$ and $n=2.0$. Compare with Fig. (4), obtained with the bond-fluctuation algorithm.

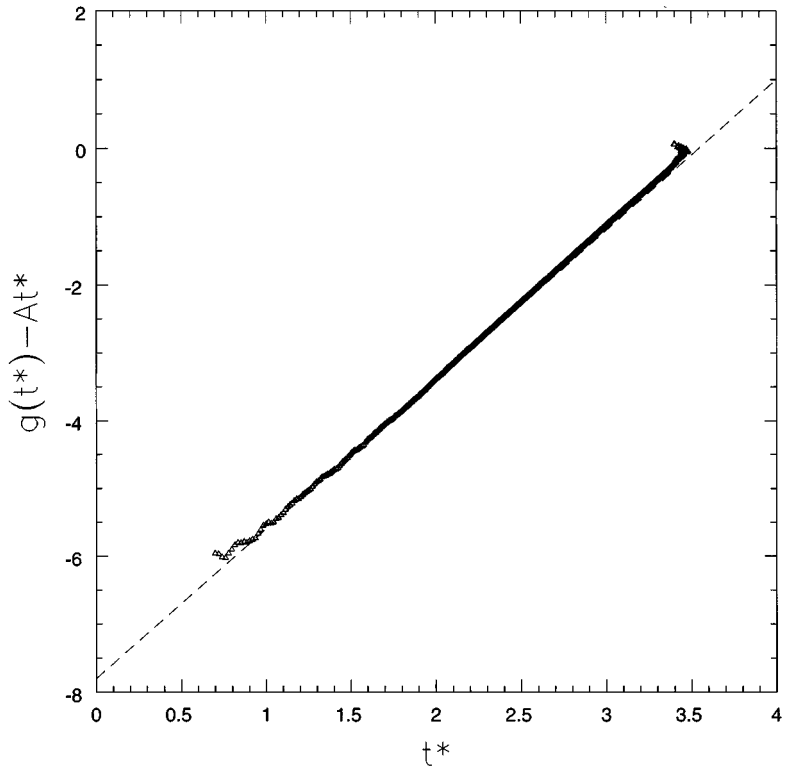

FIG. 4. Log-log plot of the difference $g(t)-At$ as a function of t for the bond-fluctuation algorithm. The exponent n in the correction Bt^n takes a value $n=2.2$; here $B=4.1\times10^{-4}$.

$e^{\chi Nt}=e^{-\beta U}$ with $\chi=\beta J$ and $\beta=1/k_BT$ as usual. For this model we can define the partial partition function of a SAW at a fixed value of t,

$$Z_N(\chi,t)=\aleph_N P_N(t)e^{\chi Nt}, \tag{33}$$

or, equivalently, the distribution

$$P_N^{(\chi)}(t)=\frac{P_N(t)e^{\chi Nt}}{\int_0^\infty P_N(t)e^{\chi Nt}dt} \tag{34}$$

at any χ. At this stage this model is merely *designed to probe* the structure and the scaling properties of $P_N(t)$. However, we showed in Ref. [10] that the mean energy of an interacting self-avoiding walk (ISAW) of radius of gyration r is equal to $-JM_N(r)$ where J is a coupling constant and where the mean number of contacts $M_N(r)$ behaves according to

$$M_N(r)=aN+b\left(\frac{r}{N^\nu}\right)^{-1/(\nu-1/d)}-C\left(\frac{r}{N^\nu}\right)^{(1-1/d)/(\nu-1/d)}-D\left(\frac{r}{N^\nu}\right)^{1/(1-\nu)}. \tag{35}$$

Hence the mean number of contacts per monomer reads

$$m_N(t)=a+bt-\frac{C}{N}(Nt)^{-\sigma}-\frac{D}{N}(Nt)^{-q}, \tag{36}$$

where $\sigma=1-1/d$ accounts for the surface correction term exponent [9], and q is given in Eq. (18). In the globule phase and for large chains, Eq. (36) reduces to

$$m_N(t)=a+bt. \tag{37}$$

It thus appears that the previous formal model $U=-NJt$ coincides with a mean-field approximation of the ISAW model.

We now show that varying the temperature T induces a *geometric* tricritical phase transition between a coil state and a globule state. As justified by the above discussion, this transition is nevertheless strongly related to the *experimental* coil-globule transition, which is generally assumed to be described by the ISAW model. Moreover, we claim that this formal transition should be the geometric basis underlying any real coil-globule transition.

It is clear from Eq. (11) that in the thermodynamic limit, t vanishes in the coil state but remains finite in the globule state, and thus appears as a possible order parameter of the coil-globule transition. Henceforth we will focus on the distribution $P_N^{(\chi)}(t)$ defined in Eq. (34). Taken into account Eqs. (29) and (31), we shall use the following expression:

$$P_N^{(\chi)}(t)=\frac{\lambda N^{1+c}t^c e^{-N(At+Bt^n)}e^{-A'(Nt)^{-q}}e^{\chi Nt}}{I_N(\chi)}, \tag{38}$$

where

$$I_N(\chi)=\int_0^{t_{max}}\lambda N^{1+c}t^c e^{-N(At+Bt^n)}e^{-A'(Nt)^{-q}}e^{\chi Nt}dt \tag{39}$$

is the normalization. For given values of N and χ, the distribution $P_N^{(\chi)}(t)$ varies with t as

$$P_N^{(\chi)}(t)\sim t^c e^{-A'(Nt)^{-q}}e^{-N[(A-\chi)t+Bt^n]}. \tag{40}$$

According to the sign of $A-\chi$, the dominant contribution to $P_N^{(\chi)}(t)$ is located in different domains of values of t.

For $\chi<A$ (high temperatures), the distribution is strongly peaked around a value of t of order $O(1/N)$. This corresponds to values of r of order $O(N^\nu)$, and leads us to identify this high-temperature regime with a *coil phase*.

For $\chi>A$ (low temperatures), $P_N^{(\chi)}(t)$ exhibits two peaks, respectively localized around $t_1\sim 1/N$ and $t_2=[(\chi-A)/nB]^{1/(n-1)}$. These two peaks are well separated, and their respective contributions are $S_1\sim N^{-(1+c)}$ and $S_2\sim e^{N(n-1)Bt_2^n}$; hence the dominant contribution comes from the vicinity of t_2. This corresponds to values of r of order $O(N^{1/d})$, and leads us to identify this low-temperature regime with a *globule phase*. Hence varying the temperature induces a phase transition whose critical point θ is given through the relationship $\chi=A$, namely,

$$\theta=\frac{J}{k_BA}. \tag{41}$$

VI. SCALING PROPERTIES OF THE GEOMETRIC COIL-GLOBULE TRANSITION

The distribution of order parameters was studied carefully by Binder [22] within a general framework; he showed a general scaling behavior (finite-size scaling analysis) in the vicinity of phase transitions according to their order. In the same spirit, we shall now describe the finite-size scaling of $P_N^{(\chi)}(t)$ around the transition temperature θ, and moreover investigate how the thermodynamic limit is reached in our specific situation.

It will appear convenient to introduce the rescaled variables

$$\hat{t}=N^{1/n}t, \tag{42}$$

$$\hat{\tau}=N^{1-1/n}\tau, \tag{43}$$

where τ is the reduced temperature difference

$$\tau=\frac{T-\theta}{T}=\frac{A-\chi}{A}. \tag{44}$$

Inserting Eqs. (42) and (43) into Eq. (38) finally gives

$$P_N^{(\chi)}(t)dt=\frac{\lambda N^{(1+c)(1-1/n)}\hat{t}^c e^{-[A\hat{\tau}\hat{t}+B\hat{t}^n]}e^{-A'N^{-q(1-1/n)}\hat{t}^{-q}}}{I_N(\chi)}d\hat{t}. \tag{45}$$

We introduce the notations

$$P_N^{(\chi)}(t)dt=\hat{P}_N(\hat{\tau},\hat{t})d\hat{t}, \tag{46}$$

$$h(\hat{\tau},\hat{t})=\hat{t}^c e^{-[A\hat{\tau}\hat{t}+B\hat{t}^n]}, \tag{47}$$

$$I_\alpha(\hat{\tau},N)=\int_0^\infty \hat{t}^\alpha h(\hat{\tau},\hat{t})e^{-A'N^{-q(1-1/n)}\hat{t}^{-q}}d\hat{t}. \quad (48)$$

This leads to the relation

$$\hat{P}_N(\hat{\tau},\hat{t})=\frac{h(\hat{\tau},\hat{t})e^{-A'N^{-q(1-1/n)}\hat{t}^{-q}}}{I_0(\hat{\tau},N)}. \quad (49)$$

A. Distribution of probability in the scaling domain and its thermodynamic limit

We now investigate the thermodynamic limit ($N\to\infty$) of the distribution $\hat{P}_N(\hat{\tau},\hat{t})$ in the domain where $\hat{t}$ and $\hat{\tau}$ remain finite, which will appear to be the scaling domain ($\hat{t}$ and $\hat{\tau}$ will actually appear to be the scaling variables of the transition). Nevertheless, due to the value of c, which happens to be $c<-1$, the limiting behavior $e^{-A'N^{-q(1-1/n)}\hat{t}^{-q}}\to 1$ cannot be cast directly in expression (48) of $I_0(\hat{\tau},N)$; in fact, the nonintegrability of the remaining integrand in $\hat{t}=0$ forbids us in that case to invert the limit and the integration. Let us stress that the value $c^*=-1$ appears as a threshold for the behavior with respect to N (at fixed $\hat{\tau}$). We first rewrite Eq. (48) for $\alpha=0$ into

$$I_0(\hat{\tau},N)=N^{-(1+c)(1-1/n)}\int_0^\infty z^c e^{-A'z^{-q}} \times e^{-N^{-(1-1/n)}A\hat{\tau}z}e^{-N^{-(n-1)}Bz^n}dz \quad (50)$$

by a mere change of variable $z=N^{(1-1/n)}\hat{t}$. For a fixed value of $\hat{\tau}$, the first step is to bound from above the factor $e^{-N^{-(1-1/n)}A\hat{\tau}z}e^{-N^{-(n-1)}Bz^n}$ with respect to z *independently of* N. This is immediate since

$$e^{-N^{-(1-1/n)}A\hat{\tau}z}e^{-N^{-(n-1)}Bz^n} = e^{-[A\hat{\tau}\hat{t}+B\hat{t}^n]} \leqslant \begin{cases} 1 & \text{if } \hat{\tau}\geqslant 0 \\ e^{(n-1)B(-A\hat{\tau}/nB)^{n/(n-1)}} & \text{if } \hat{\tau}<0. \end{cases} \quad (51)$$

Now because $c<-1$, the partial integrand $z^c e^{-A'z^{-q}}$ in Eq. (50) is integrable. Thanks to the Lebesgue theorem, it is then legitimate to take the thermodynamic limit inside the integral appearing in Eq. (50), which leads to

$$I_0(\hat{\tau},N)\approx N^{-(1+c)(1-1/n)}\int_0^\infty z^c e^{-A'z^{-q}}dz = C_0(A')N^{-(1+c)(1-1/n)}. \quad (52)$$

Explicit calculation of this integral is possible, leading to

$$C_0(A')=\frac{1}{q}\Gamma\left[\frac{-(1+c)}{q}\right](A')^{(1+c)/q}. \quad (53)$$

We note that this leading order only depends on A' but not on $\hat{\tau}$ or N in the scaling domain. Hence $\hat{P}_N(\hat{\tau},\hat{t})$ writes

$$\hat{P}_N(\hat{\tau},\hat{t})=N^{(1+c)(1-1/n)}\frac{h(\hat{\tau},\hat{t})e^{-A'N^{-q(1-1/n)}\hat{t}^{-q}}}{C_0(A')}, \quad (54)$$

where the factor $e^{-A'N^{-q(1-1/n)}\hat{t}^{-q}}$ can be ignored (we remind the reader that in the scaling domain, $\hat{t}$ and $\hat{\tau}$ remain finite when $N\to\infty$), so that $\hat{P}_N(\hat{\tau},\hat{t})$ reduces in the scaling domain to

$$\hat{P}_N(\hat{\tau},\hat{t})=N^{(1+c)(1-1/n)}\frac{h(\hat{\tau},\hat{t})}{C_0(A')}. \quad (55)$$

As before, care must be taken when computing the normalization $I_0(\hat{\tau},N)$ of $\hat{P}_N(\hat{\tau},\hat{t})$; actually, it must be performed on the overall expression (29) in order to handle correctly the integration in the vicinity of $\hat{t}=0$. This explains the remaining power of N in Eq. (55), which does not exist in Binder's expression [22], however identical in any other respect.

B. Thermodynamic limit of the moments of $\hat{P}_N(\hat{\tau},\hat{t})$

We now come to the computation of the various moments of the rescaled order parameter $\hat{t}$. Let α be an arbitrary real number; intending to give an explicit expression for

$$\langle\hat{t}^\alpha\rangle(\hat{\tau})=\int_0^\infty \hat{t}^\alpha\hat{P}_N(\hat{\tau},\hat{t})d\hat{t}=\frac{I_\alpha(\hat{\tau},N)}{I_0(\hat{\tau},N)}, \quad (56)$$

we have to distinguish two cases according to the position of $\alpha+c$ with respect to -1.

(i) $\alpha+c>-1$: in this case we use expression (48). Due to the integrability of the partial integrand $\hat{t}^{c+\alpha}e^{A\hat{\tau}\hat{t}+B\hat{t}^n}$ all over the integration domain and because the factor $e^{-A'N^{-q(1-1/n)}\hat{t}^{-q}}\leqslant 1$ on that domain, we are allowed to take the thermodynamic limit inside the integral. This leads to

$$I_\alpha(\hat{\tau},N)\sim J_\alpha(\hat{\tau}), \quad (57)$$

where

$$J_\alpha(\hat{\tau})=\int_0^\infty \hat{t}^{c+\alpha}e^{-(A\hat{\tau}\hat{t}+B\hat{t}^n)}d\hat{t}. \quad (58)$$

Hence

$$\langle\hat{t}^\alpha\rangle(\hat{\tau})=N^{(1+c)(1-1/n)}\frac{J_\alpha(\hat{\tau})}{C_0(A')}. \quad (59)$$

We note that this amounts to making direct use of Eq. (55) in the computation of the moments. It is possible to give a closed form of $J_\alpha(\hat{\tau})$ in the limit where $\hat{\tau}\gg 1$,

$$J_\alpha(\hat{\tau})\approx(A\hat{\tau})^{-(\alpha+c+1)}\Gamma(\alpha+c+1). \quad (60)$$

In the case $\hat{\tau}<0$ and $|\hat{\tau}|\gg 1$, the standard steepest-descent method allows us to approximate

$$J_\alpha(\hat{\tau})\approx\left(\frac{2\pi}{n(n-1)B}\right)^{1/2}\left(\frac{-A\hat{\tau}}{nB}\right)^{(c+\alpha)/(n-1)} \times e^{(n-1)B(-A\hat{\tau}/nB)^{n/(n-1)}}. \quad (61)$$

(ii) $\alpha+c<-1$: in this case, we have to start from the equivalent expression

$$I_\alpha(\hat{\tau},N)=N^{-(1+c+\alpha)(1-1/n)} \times\int_0^\infty z^{c+\alpha}e^{-N^{-(1-1/n)}A\hat{\tau}z+N^{-(n-1)}Bz^n}e^{-A'z^{-q}}dz. \tag{62}$$

The procedure already used in the computation of $I_0(\hat{\tau},N)$ [Eq. (50)] can be extended straightforwardly to the present situation, leading for a fixed value of $\hat{\tau}$ (hence inside the scaling domain) to

$$I_\alpha(\hat{\tau},N)=N^{-(1+c+\alpha)(1-1/n)}C_\alpha(A'), \tag{63}$$

where

$$C_\alpha(A')\approx\int_0^\infty z^{c+\alpha}e^{-A'z^{-q}}dz=\frac{1}{q}\Gamma\left[\frac{-(1+c+\alpha)}{q}\right] \times(A')^{(1+c)/q} \tag{64}$$

no longer depends on $\hat{\tau}$. This finally leads to the desired result

$$\langle\hat{t}^\alpha\rangle(\hat{\tau})=\frac{N^{-(1+c+\alpha)(1-1/n)}C_\alpha(A')}{N^{-(1+c)(1-1/n)}C_0(A')}=N^{-\alpha(1-1/n)}\frac{C_\alpha(A')}{C_0(A')}, \tag{65}$$

or, equivalently, for the initial order parameter t,

$$\langle t^\alpha\rangle(\hat{\tau})=N^{-\alpha}\frac{C_\alpha(A')}{C_0(A')}. \tag{66}$$

Let us notice that in this case where $\alpha+c<-1$, the truncated expression of the probability distribution given in Eq. (55) does not suffice to obtain the value of the moments.

VII. DISCUSSION OF THE TRICRITICAL NATURE OF THE GEOMETRIC COIL-GLOBULE TRANSITION AND CALCULATION OF THE CRITICAL EXPONENTS

It was shown in Sec. V that t is a suitable order parameter for the coil-globule transition. Actually, any positive power t^α of t would be equally convenient, insofar as in the thermodynamic limit, t^α would be equal to zero in the coil state and strictly positive in the globule state. In order to convince the reader of the importance of the position of c with respect to the threshold value $c^*=-1$, we first present the rather straightforward scaling picture that occurs for $c>-1$, before examining the relevant situation $c<-1$.

A. Standard tricritical scaling behavior when $c>-1$

Let us suppose here that $c>-1$ and let α be some strictly positive real number. As stated above, the moment $\langle t^\alpha\rangle$ appears to be a macroscopic order parameter characterizing the phase (coil or globule) in the thermodynamic limit; its rescaled form $\langle\hat{t}^\alpha\rangle$ behaves with respect to the rescaled control parameter $\hat{\tau}$ in the vicinity of the phase transition ($\hat{\tau}=0$) as [see Eq. (58)]

$$\langle\hat{t}^\alpha\rangle=\frac{J_\alpha(\hat{\tau})}{J_0(\hat{\tau})}, \tag{67}$$

where

$$J_0(\hat{\tau})=\int_0^\infty\hat{t}^c e^{-(A\hat{\tau}\hat{t}+B\hat{t}^n)}d\hat{t} \tag{68}$$

is now well defined since $c>-1$. In the case $\alpha=1$, this leads to

$$\langle\hat{t}\rangle\sim\begin{cases}\hat{\tau}^{-1} & \text{if } \hat{\tau}>0\\ |\hat{\tau}|^{1/(n-1)} & \text{if } \hat{\tau}<0.\end{cases} \tag{69}$$

In order to interpret this scaling law in the language of polymer physics, we introduce the quantity

$$R_G^*=N^{1/d}\langle t\rangle^{-(\nu-1/d)}, \tag{70}$$

which is the most relevant definition of the radius of gyration in terms of the order parameter $\langle t\rangle$. The usual definition (denoted R_G in Sec. I) would involve the mean value $\langle t^{-2(\nu-1/d)}\rangle^{1/2}$ of a negative power of t which has not the behavior of an order parameter. From Eqs. (69) and (70), we obtain

$$R_G^*=N^{\nu_\theta}\langle\hat{t}\rangle^{-(\nu-1/d)}\sim\begin{cases}N^{\nu_\theta}\hat{\tau}^{\nu-1/d} & \text{if } \hat{\tau}>0\\ N^{\nu_\theta}|\hat{\tau}|^{-[1/(n-1)](\nu-1/d)} & \text{if } \hat{\tau}<0,\end{cases} \tag{71}$$

where

$$\nu_\theta=\frac{1}{d}+\frac{1}{n}\left(\nu-\frac{1}{d}\right). \tag{72}$$

We verify that ν_θ satisfies the hyperscaling relations

$$\nu-\frac{1}{d}=\frac{\nu-\nu_\theta}{\phi}\quad\text{and}\quad-\frac{1}{n-1}\left(\nu-\frac{1}{d}\right)=\frac{\frac{1}{d}-\nu_\theta}{\phi} \tag{73}$$

where the crossover exponent ϕ is equal to

$$\phi=1-1/n. \tag{74}$$

This hyperscaling relation means that

$$R_G^*\sim\begin{cases}N^\nu & \text{if } \hat{\tau}>0\\ N^{1/d} & \text{if } \hat{\tau}<0.\end{cases} \tag{75}$$

It thus clearly appears that R_G^* satisfies a standard [1] tricritical scaling law $R_G^*\sim N^{\nu_\theta}f(N^\phi\tau)$, so that the rescaled variable $\hat{\tau}=N^\phi\tau$ is precisely one of the scaling variable of the transition. We stress that the exponents appearing in this scaling law do not depend on the value of c, provided $c>-1$; hence in particular they remain valid in the case where no factor t^c is present in the distribution $P_N(t)$ (i.e., $c=0$).

B. Anomalous tricritical scaling behavior for the observed situation $c<-1$

We now turn to the observed case $c<-1$. Due to the divergence in $t=0$ of the factor t^c discussed at length in Sec. VI, the mean value $\langle\hat{t}\rangle$ now writes according to Eq. (59),

$$\langle\hat{t}\rangle = N^{(1+c)(1-1/n)}\frac{J_1(\hat{\tau})}{C_0(A')}, \tag{76}$$

so that R_G^* now writes

$$R_G^* = N^{\overline{\nu}_\theta} H(\hat{\tau}), \tag{77}$$

with

$$\overline{\nu}_\theta = \frac{1}{d} + \left[\frac{1}{n} - (1+c)\left(1-\frac{1}{n}\right)\right]\left(\nu - \frac{1}{d}\right) \tag{78}$$

and

$$H(\hat{\tau}) \sim \left(\frac{J_1(\hat{\tau})}{C_0(A')}\right)^{-(\nu-1/d)}. \tag{79}$$

In view of Eqs. (60) and (61),

$$R_G^* \sim \begin{cases} N^{\overline{\nu}_\theta}\hat{\tau}^{(2+c)(\nu-1/d)} & \text{if } \hat{\tau}>0 \\ N^{\overline{\nu}_\theta}|\hat{\tau}|^{-[(1+c)(n-1)](\nu-1/d)} e^{-(\nu-1/d)(n-1)B(-A\hat{\tau}/nB)^{n/(n-1)}} & \text{if } \hat{\tau}<0, \end{cases} \tag{80}$$

where it is implicitly assumed that $|\hat{\tau}|\gg 1$. The exponent $\overline{\nu}_\theta$ still satisfies the expected hyperscaling law

$$(2+c)\left(\nu - \frac{1}{d}\right) = \frac{\nu - \overline{\nu}_\theta}{\phi} \tag{81}$$

on the coil side of the transition ($\hat{\tau}>0$) but not on the globule side ($\hat{\tau}<0$). On this globule side,

$$\frac{\frac{1}{d} - \overline{\nu}_\theta}{\phi} = \left(1 + c - \frac{1}{n-1}\right)\left(\nu - \frac{1}{d}\right), \tag{82}$$

whereas the right-hand member of this equation should be $-[1+c/(n-1)](\nu-1/d)$ according to the expression of R_G^* in the case $\hat{\tau}<0$ [Eq. (80)]. This anomalous hyperscaling law stems from the unusual exponential behavior appearing on the globule side of this transition. It must be stressed that in the case $c<-1$, the factor t^c controls the value of the critical exponents. Moreover, a strong discontinuity arises in the behavior of R_G^* when crossing the threshold value $c^*=-1$ (in the globule regime $\hat{\tau}<0$). Let us finally remark that this threshold value $c^*=-1$ is robust, since it would be similarly obtained when taking any positive power t^α instead of t for the order parameter; more precisely, expressing the distribution in variable $z=t^\alpha$ would lead to a factor $z^{(c+1+\alpha)/\alpha}$, where the new exponent $c_\alpha=(c+1+\alpha)/\alpha$ satisfies $c_\alpha<-1$ if and only if $c<-1$.

VIII. NUMERICAL REALITY VERSUS THERMODYNAMIC LIMIT

In order to link the above thermodynamic analysis and numerical data, we shall now investigate the manner and the rate at which the thermodynamic limit is reached. This rate will appear to be so slow that, for some quantities, we shall have to distinguish two regimes, referred to as (TL) for the thermodynamic limit and (NUM) for the finite-size regime.

A. Numerical evaluation of $I_\alpha(\hat{\tau},N)$

We now intend to compute $I_\alpha(\hat{\tau},N)$ for any finite value of N, especially for the small values $N<200$ relevant for our simulations. It appears essential to distinguish two cases according to the sign of $\hat{\tau}$.

(i) Whenever $\hat{\tau}>0$, the integrand involved in the definition of $I_\alpha(\hat{\tau},N)$ [Eq. (48)] exhibits a lonely peak and is uniformly bounded with respect to N (in both cases $\alpha+c>-1$ and $\alpha+c<-1$); this allows us not only to take the thermodynamic limit inside the integral but also to estimate the rate of convergence in the limit as $N\to\infty$. The explicit computation depends on the sign of $\alpha+c+1$; nevertheless, in both cases $\alpha+c>-1$ and $\alpha+c<-1$, provided $\hat{\tau}>0$, the integral $I_\alpha(\hat{\tau},N)$ converges toward its thermodynamic limit fast enough to identify the numerical regime with the asymptotic one.

(ii) We now turn to the case $\hat{\tau}<0$. It appears convenient to split the integrand into two factors. For sufficiently large values of $|\hat{\tau}|$, the first one $e^{-(A\hat{\tau}\hat{t}+B\hat{t}^n)}$ is peaked around the value

$$\hat{t}_0 = \left(\frac{-A\hat{\tau}}{nB}\right)^{1/(n-1)}, \tag{83}$$

and its height does not depend on N. In the case $\alpha+c<-1$, we denote $\tilde{J}_\alpha(\hat{\tau})$ the contribution of this peak to the integral $I_\alpha(\hat{\tau},N)$. In the case $\alpha+c>-1$, it is possible to identify this contribution with the convergent integral $J_\alpha(\hat{\tau})$ given in Eq. (58). In both cases, the contribution remains finite and standard steepest-descent method applies (for $|\hat{\tau}|$ sufficiently large), leading to the explicit estimation

$$\left.\begin{array}{ll} \text{if } & \alpha+c>-1, \quad J_\alpha(\hat{\tau}) \\ \text{if } & \alpha+c<-1, \quad \tilde{J}_\alpha(\hat{\tau}) \end{array}\right\} \approx \left(\frac{2\pi}{n(n-1)B}\right)^{1/2}\left(\frac{-A\hat{\tau}}{nB}\right)^{(c+\alpha)/(n-1)} \times e^{(n-1)B(-A\hat{\tau}/nB)^{n/(n-1)}}. \tag{84}$$

The second factor in the integrand is $\hat{t}^{c+\alpha}e^{-A'N^{-q(1-1/n)}\hat{t}^{-q}}$;

it is peaked around $\hat{t}=0$ and gives a contribution $K_\alpha(N)$ independent of $\hat{\tau}$ varying with N according to

$$K_\alpha(N)=\int_0^\infty \hat{t}^{c+\alpha}e^{-A'N^{-q(1-1/n)}\hat{t}^{-q}}d\hat{t}$$
$$=N^{-(1+c+\alpha)(1-1/n)}C_\alpha(A'). \tag{85}$$

For $|\hat{\tau}|\gg 1$, the two peaks are well separated, so that

$$I_\alpha(\hat{\tau},N)=\begin{cases} J_\alpha(\hat{\tau})+K_\alpha(N) & \text{if } \alpha+c>-1 \\ \widetilde{J}_\alpha(\hat{\tau})+K_\alpha(N) & \text{if } \alpha+c<-1. \end{cases} \tag{86}$$

Focusing on $I_0(\hat{\tau},N)$, we now want to evaluate the relative contributions of the two peaks that contribute to its integrand. As this integrand is, up to some normalization constant, equal to $\hat{P}_N(\hat{\tau},\hat{t})$, the analysis will rely on the estimation of the different contributions in $\hat{P}_N(\hat{\tau},\hat{t})$, whose relative importance is shown in Fig. 5 for various values of N. Figure 6 presents the level curves of the ratio $K_0(N)/J_0(\hat{\tau})$ in the $(\hat{\tau}-N)$ space, leading us to discriminate the domain of validity of TL from the regime where NUM presented just above holds. In conclusion, $K_\alpha(N)$ is negligible with respect to, respectively, $J_\alpha(\hat{\tau})$ or $\widetilde{J}_\alpha(\hat{\tau})$ in the numerical regime (see Table V for a comparative summary of all the results). This leads to the following estimation, valid whatever α is (provided $\hat{\tau}<0$):

$$I_\alpha(\hat{\tau},N)\approx\left(\frac{2\pi}{n(n-1)B}\right)^{1/2}\left(\frac{-A\hat{\tau}}{nB}\right)^{(c+\alpha)/(n-1)}$$
$$\times e^{(n-1)B(-A\hat{\tau}/nB)^{n/(n-1)}}. \tag{87}$$

It is now clear that in this case $\alpha+c<-1$, and especially for $\alpha=0$, the thermodynamic limit of $I_\alpha(\hat{\tau},N)$ will never be reached in numerical simulations.

B. Numerical evaluation of the distribution $\hat{P}_N(\hat{\tau},\hat{t})$ and of its moments

We first evaluate the leading behavior of the distribution $\hat{P}_N(\hat{\tau},\hat{t})$ given in Eq. (49) when restricting to the numerical regime. In that regime, we have seen that $I_0(\hat{\tau},N)\approx\widetilde{J}_0(\hat{\tau})$, so that

$$\hat{P}_N(\hat{\tau},\hat{t})=\frac{h(\hat{\tau},\hat{t})e^{-A'N^{-q(1-1/n)}\hat{t}^{-q}}}{\widetilde{J}_0(\hat{\tau})}. \tag{88}$$

For $|\hat{\tau}|$ sufficiently large we may now write explicitly the expression of the various moments on the basis of Eqs. (56) and (87)

$$\langle\hat{t}^\alpha\rangle=\frac{\widetilde{J}_\alpha(\hat{\tau})}{\widetilde{J}_0(\hat{\tau})}\sim\left(\frac{-\hat{\tau}}{nB}\right)^{\alpha/(n-1)}, \tag{89}$$

valid whatever α is. All the discussion of both the thermodynamic and the numerical regimes (for $\hat{\tau}<0$) is summarized in a comparative way in Table V.

C. Effective numerical exponents

We finally come to the expression of the numerically observable scaling laws. For $\hat{\tau}>0$, the thermodynamic limit given in Sec. VII [Eq. (80)] is relevant for the numerical analysis, namely,

$$R_G^*\sim N^{\overline{\nu}_\theta}\hat{\tau}^{(2+c)(\nu-1/d)}. \tag{90}$$

Conversely, for $\hat{\tau}<0$, taken into account Eq. (89) for $\alpha=1$, we obtain

$$R_G^*\sim N^{\nu_\theta}|\hat{\tau}|^{-(1/n-1)[\nu-(1/d)]} \tag{91}$$

in the same way as for the case $c>-1$ [Eq. (72)]. We thus may summarize the tricritical scaling behavior observed in the numerical regime (that is, for chains of lengths $N<10^{20}$).

$$R_G^*\sim\begin{cases} N^{\overline{\nu}_\theta}\hat{\tau}^{(2+c)[\nu-(1/d)]} & \text{if } \hat{\tau}>0 \\ N^{\nu_\theta}|\hat{\tau}|^{-[1/(n-1)][\nu-(1/d)]} & \text{if } \hat{\tau}<0. \end{cases} \tag{92}$$

This behavior is anomalous in the sense that there are now two different exponents ν_θ and $\overline{\nu_\theta}$. Note that, accordingly, there are two different hyperscaling relations holding, respectively, for ν_θ and $\overline{\nu_\theta}$

$$(2+c)\left(\nu-\frac{1}{d}\right)=\frac{\nu-\overline{\nu_\theta}}{\phi},$$
$$-\left(\frac{1}{n-1}\right)\left(\nu-\frac{1}{d}\right)=\frac{\frac{1}{d}-\nu_\theta}{\phi}. \tag{93}$$

TABLE V. Quantitative comparison of the thermodynamic and numerical regimes intending to summarize the analysis presented in Secs. VI, VII, and VIII (for $\hat{\tau}<0$). Here $\hat{t}_0=(-A\hat{\tau}/nB)^{1/n-1}$ [see Eq. (83)].

	TL		
	$\alpha+c<-1$	$\alpha+c>-1$	NUM
$I_\alpha(\hat{\tau},N)$	$N^{(1+c+\alpha)(1-1/n)}C_\alpha(A')$	$\sim\hat{t}_0^{(c+\alpha)}e^{(n-1)B\hat{t}_0^n}$	$\sim\hat{t}_0^{(c+\alpha)}e^{(n-1)B\hat{t}_0^n}$
$\langle\hat{t}^\alpha\rangle(\hat{\tau})$	$N^{-\alpha(1-1/n)}\dfrac{C_\alpha(A')}{C_0(A')}$	$N^{(1+c)(1-1/n)}\dfrac{I_\alpha(\hat{\tau})}{C_0(A')}$	$\sim\hat{t}_0^\alpha$
$I_0(\hat{\tau},N)$	$N^{(1+c)(1-1/n)}C_0(A')$		$\sim\hat{t}_0^c e^{(n-1)B\hat{t}_0^n}$
$\hat{P}_N(\hat{\tau},\hat{t})$	$\dfrac{N^{(1+c)(1-1/n)}h(\hat{\tau},\hat{t})}{C_0(A')}$	(see Fig. 5)	$\dfrac{h(\hat{\tau},\hat{t})}{I_0(\hat{\tau})(\hat{\tau})}$

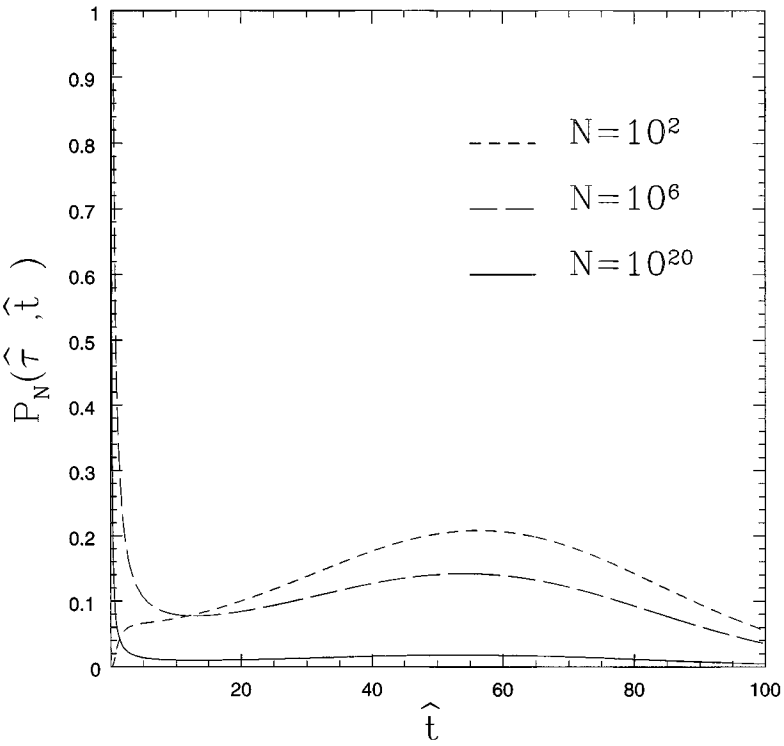

FIG. 5. Analytic plot of the normalized distribution $\hat{P}_N(\hat{\tau},\hat{t})$ according to Eq. (54) showing the relative contributions of the two peaks of the integrand of Eq. (48) (for $\alpha=0$) for increasing values of N and for $\hat{\tau}=-5$, which justifies the computation of the thermodynamic limit of the normalization factor $I_N(\chi)=\lambda N^{(1+c)(1-1/n)-\alpha/n} I_0(\hat{\tau},N)$. [Note that the areas under the three curves are equal because of the huge peak of $\hat{P}_N(\hat{\tau},\hat{t})$ in the vicinity of $\hat{t}=0$.]

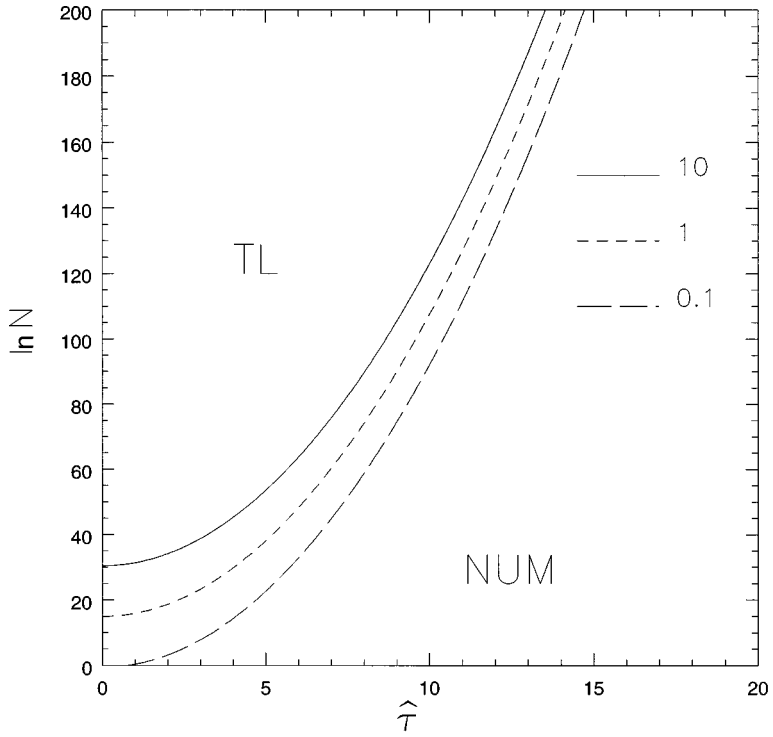

FIG. 6. $\hat{\tau}-N$ diagram showing the domains of validity of the analysis presented in Sec. VIII. Three level curves corresponding respectively to the values 0.1, 1, and 10 of the ratio $K_0(N)/J_0(\hat{\tau})$ are drawn. Above the curve of level 10, the thermodynamic limit regime (TL) is reached and Eqs. (52) and (55) are valid. The domain below the curve of level 0.1, which is nearly entirely embedded in the domain reachable numerically (namely $N<10^5$) is described by equations given in the column NUM of Table V.

The crossover exponent ϕ is identical in both hyperscaling relations, equal to $\phi=1-1/n$.

IX. ANALYSIS OF THE NUMERICAL DATA

All the above analysis provides the theoretical framework for validating the proposed structure of the distribution $P_N(t)$, and for estimating the numerical values of its parameters. In order to circumvent the numerical difficulties induced by the anomalous factor t^c, we propose the following alternative to the well-known Binder's reduced fourth cumulant [which we recall to be $U_L=3-(\langle t^4\rangle/\langle t^2\rangle^2)$]

$$Q_{\rm exp}(\chi,N)\equiv\frac{\langle t^4\rangle\langle t\rangle^2}{\langle t^2\rangle^3}, \tag{94}$$

which is directly accessible from our numerical data. According to Eq. (56), this quantity theoretically reads

$$Q(\hat{\tau},N)=\frac{I_4(\hat{\tau},N)I_1^2(\hat{\tau},N)}{I_2^3(\hat{\tau},N)}. \tag{95}$$

(i) The great advantage in introducing this new quantity is to get rid of $I_0(\hat{\tau},N)$ which does not behave similarly in the thermodynamic and numerical regimes. Indeed, in view of the results presented in Table V, the first remarkable property of Q is that it reduces in the numerical domain (which we recall to be the domain relevant for the interpretation of the numerical data) to

$$Q^{\rm NUM}(\hat{\tau})=\frac{J_4(\hat{\tau})J_1^2(\hat{\tau})}{J_2^3(\hat{\tau})}. \tag{96}$$

Let us stress that $Q^{\rm NUM}$ no longer depends on N, nor on A', nor on λ.

(ii) Moreover, at the transition point, namely, when $\hat{\tau}=0$, the quantities $J_\alpha(\hat{\tau}=0)$ $(\alpha=1,2,4)$ involved in $Q^{\rm NUM}$ are equal to

$$J_\alpha(\hat{\tau}=0)=\frac{1}{n}\Gamma\left(\frac{\alpha+c+1}{n}\right)B^{-(\alpha+c+1)/n}, \tag{97}$$

so that

$$Q_\theta\equiv Q^{\rm NUM}(\hat{\tau}=0)=\frac{\Gamma\left(\frac{5+c}{n}\right)\left[\Gamma\left(\frac{2+c}{n}\right)\right]^2}{\left[\Gamma\left(\frac{3+c}{n}\right)\right]^3}. \tag{98}$$

Coming back to the bare variable χ, instead of $\hat{\tau}$ which depends on our knowledge of A and of n, we draw in Fig. 7 the curves $Q_{\rm expt}(\chi,N)$, representing Q as a function of χ for different values of N. Due to the fact that Q_θ does not depend on N [Eq. (98)], all these curves are theoretically meant to cross in a unique point, appearing to be the transition point $\chi=A$, which is accurately verified on the numerical curves (see Fig. 7). Note that this procedure for obtaining A does not require any previous knowledge of the other parameters (A', λ, B, and c).

(iii) A third fruitful property of Q is that it gives a direct access to the value of c. As a matter of fact, Q is a decreasing function of χ, then is maximal in $\chi=0$, which corresponds to $\hat{\tau}\to\infty$ and makes it possible to use Eq. (60), which leads to

$$Q_{\rm max}=\frac{(4+c)(3+c)}{(2+c)^2}, \tag{99}$$

whose remarkable feature is to depend exclusively on c and to be quickly decreasing around $c^*=-1$. In consequence, this controls in a very efficient way the numerical estimation of the value of c. Figure 7 clearly shows that $c<-1$, in fact that $c<-1.07$ which is compatible with the theoretical interval obtained using Eq. (27) and with the numerical value previously obtained in Sec. IV.

(iv) A last interest of this quantity $Q(\hat{\tau})$ is that its slope at the transition point gives access to B through the following expression:

$$\frac{Q'(\hat{\tau}=0)}{Q(\hat{\tau}=0)}=B^{-1/n}\left[3\frac{\Gamma\left(\frac{4+c}{n}\right)}{\Gamma\left(\frac{3+c}{n}\right)}-2\frac{\Gamma\left(\frac{3+c}{n}\right)}{\Gamma\left(\frac{2+c}{n}\right)}-\frac{\Gamma\left(\frac{6+c}{n}\right)}{\Gamma\left(\frac{5+c}{n}\right)}\right]. \tag{100}$$

As displayed in Figure 8, the curves $Q^{\rm NUM}(\hat{\tau})$ collapse onto a universal one for $n=2.1\pm0.1$. This value is consistent with the value of n given by Eq. (98). We also note in Fig. 8 that $Q_{\rm expt}(\chi=\infty)\approx1$ (corresponding to $\hat{\tau}=-\infty$) as expected. The whole set of numerical values of the parameters of $P_N(t)$ is given in Table IV.

Focusing on the transition point ($\hat{\tau}=0$), we draw in Figs. 9, 10 and 11, respectively, the numerical curves

$$\hat{t}\to\frac{t^\alpha P_N(t)e^{ANt}e^{A'(Nt)^{-q}}}{\lambda N^{1+c-[(\alpha+c)/n]}}, \quad \alpha=0,1,2 \tag{101}$$

for different values of N. For each value of $\alpha=0$, 1, or 2, the curves collapse as expected on the universal one $\hat{t}\to\hat{t}^\alpha h(\hat{\tau}=0,t)=\hat{t}^{\alpha+c}e^{-B\hat{t}^n}$ which concludes the validation of our theoretical predictions and comforts the numerical values given in Table IV.

Figure 9 (for $\alpha=0$) clearly evidences the divergence due to the factor t^c. Figure 10 (for $\alpha=1$) still exhibiting a divergence in $\hat{t}=0$ supports once more that $c<-1$. Figure 11 (for $\alpha=2$) highlights the domain where the value of B is sensitive.

Finally, we may now give improved values for ν_θ, $\overline{\nu_\theta}$ and ϕ using the best values of n and c given in Table IV and $\nu=0.588$:

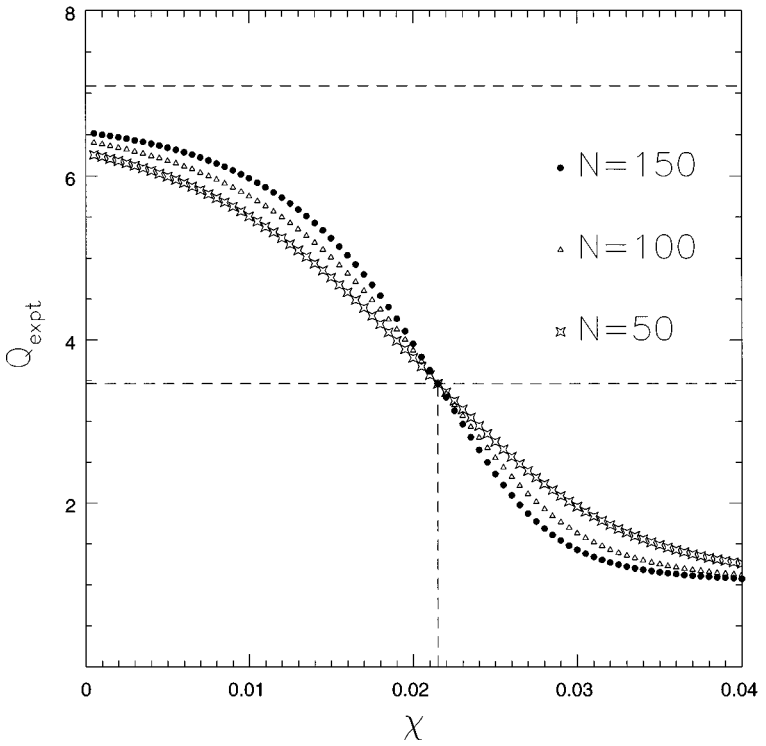

FIG. 7. Generalized cumulant Q_{expt} defined in Eq. (94), as a function of χ. The three curves corresponding to values of $N=50$, 100, 150 intersect in a single point ($\chi=\chi_\theta$, $Q=Q_\theta$) with $\chi_\theta=A$. This gives access to the numerical value of $A=0.0215\pm0.0005$. Q_θ is given in Eq. (98). For $c=-1.07$, $Q_{\max}=6.54$ according to Eq. (99). Note that the observed value of $Q_{\text{expt}}(\chi=0)$ for $N=150$ is very close and obviously provides a lower bound for $Q_{\max}$. For the best value $c=-1.13$, $Q_{\max}=7.09$, which corresponds to the upper dashed line.

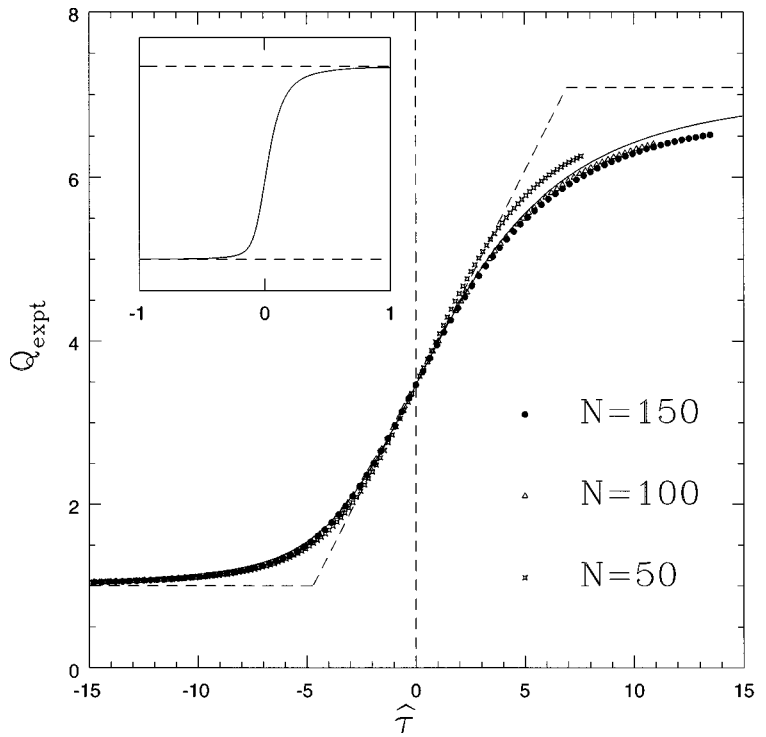

FIG. 8. Same as Fig. 7, but using the rescaled variable $\hat{\tau}$ for $n=2$. The three curves obtained for $N=50$, 100, and 150 now collapse. The dashed line accounts for the slope at $\hat{\tau}=0$ and for the asymptotic values of Q: $Q_{\text{expt}}(\chi=\infty)=1$ ($\hat{\tau}=-\infty$) and $Q_{\text{expt}}(\chi=0)=7.09$ ($\hat{\tau}=+\infty$). The inset displays a sketch of $Q(\hat{\tau})$ in the thermodynamic limit.

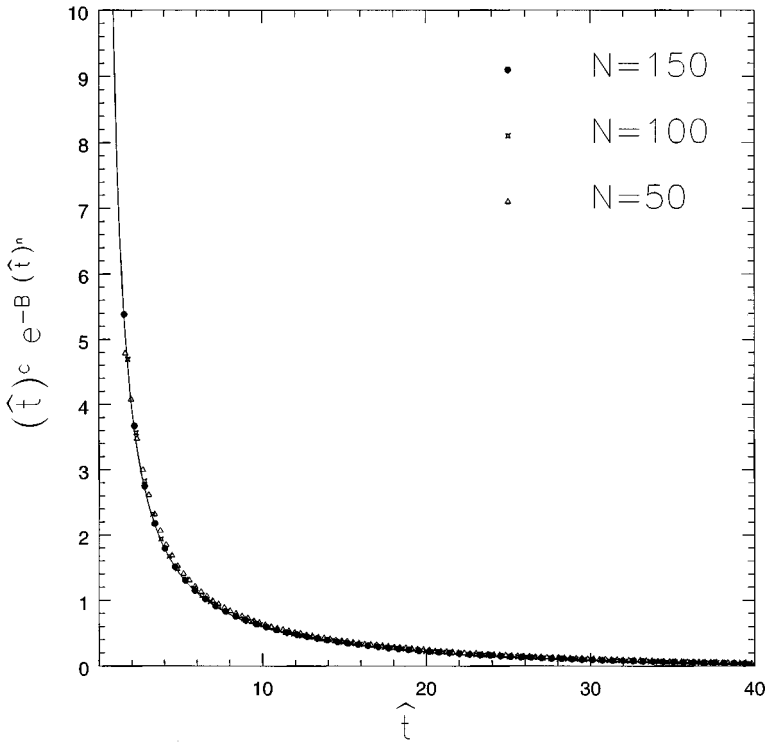

FIG. 9. Numerical analysis corresponding to Eq. (101) with $\alpha=0$ for three different chain lengths $N=50$, 100, and 150. The plain line is the theoretical prediction.

$$\nu_\theta = 0.455 \pm 0.006,$$
$$\overline{\nu_\theta} = 0.472 \pm 0.008, \qquad (102)$$
$$\phi = 0.48 \pm 0.02.$$

X. CONCLUSION

In this paper we have presented a phenomenological approach to the statistics of a self-avoiding walk, relying on a numerical simulation. We showed a relevant order parameter t on which a geometric coil-globule transition is perceived

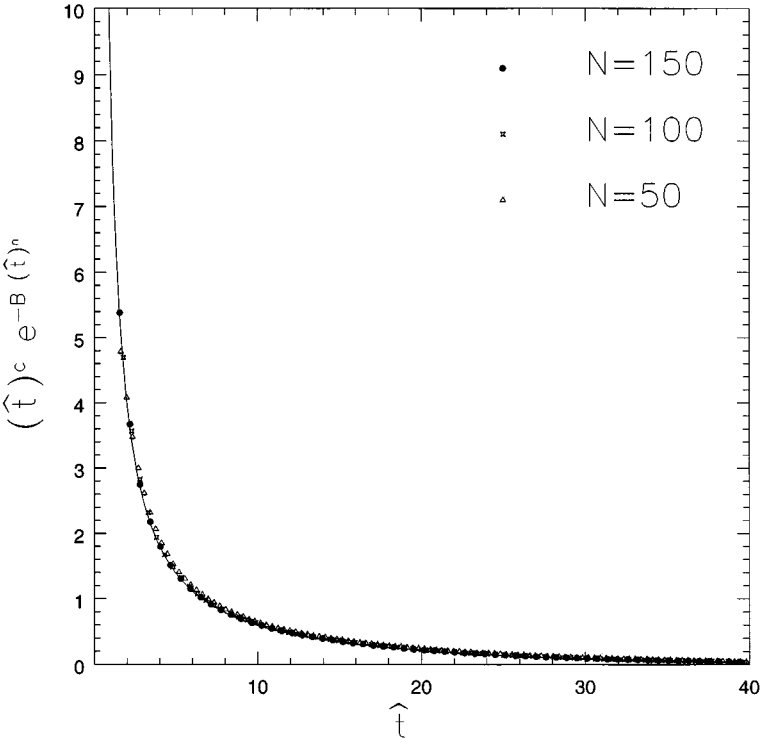

FIG. 10. Same as Fig. 9 but for $\alpha=1$ in Eq. (101).

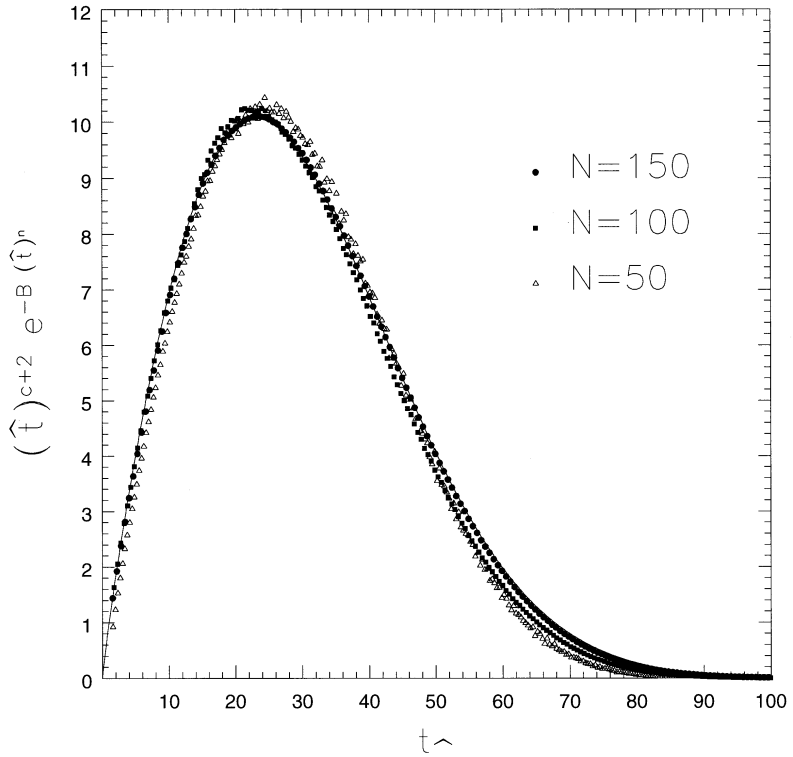

FIG. 11. Same as Fig. 9, but for $\alpha=2$ in Eq. (101).

when adding a formal Boltzmann factor; let us recall that this factor intends to weight differently the corresponding subspaces of conformations (coil or globule) when the temperature is varied. Such an intrinsic transition allows us to give a precise meaning to the coil and the globule phases. We have identified and modeled the different contributions exhibited by our numerical results, which allowed us to reconstruct the distribution $P_N(t)$ of the order parameter t. We have exhibited an unexpected contribution t^c to $P_N(t)$, and we related the associated exponent c to the well-known enhancement exponents in the coil and the globule phases. We showed the scaling variables $\hat{\tau}$ and $\hat{t}$ of the transition, and derived the corresponding scaling laws. It has been proven that a threshold value $c^*=-1$ separates two qualitatively different scaling behaviors, namely, a standard tricritical behavior for $c>c^*$ and an anomalous scaling for $c<c^*$ in the thermodynamic limit; the latter case $c<-1$ is the observed situation. An additional consequence of this value $c<-1$ is the dramatically slow rate of convergence toward the thermodynamic limit, which imposes an effective regime (the so-called ''numerical regime'' relying on finite-size scaling) in order to interpret the numerical data correctly [23].

All the difficulties encountered in the numerical analysis stem from the anomalous value $c<-1$; we expect that these problems might remain in more physical situations. In order to circumvent such problems, the numerical analysis could take advantage of the extended cumulant Q introduced in Sec. IX. We also suggest that R_G^* introduced in Sec. VII might be an interesting alternative quantity more convenient than the usual radius of gyration R_G recalled in Sec. I.

We claim that the various contributions appearing in the structure of $P_N(t)$ provide the geometric basis underlying physical coil-globule transitions, in the sense where it describes the influence of both the topology of the chain and the self-avoiding constraints. The way of implementing the geometric description in a real situation, through a factorization procedure, has been tackled in a preceding paper [19], and will be soon extensively exposed by the authors.

[1] P. G. de Gennes, J. Phys. (France) Lett. **36**, L-55 (1975); **39**, L-299 (1978).
[2] See for example, C. Vanderzande, A. L. Stella, and F. Seno, Phys. Rev. Lett. **67**, 2757 (1991); B. Duplantier and H. Saleur, *ibid.* **61**, 1521 (1988); **62**, 1368 (1989).
[3] B. Duplantier and H. Saleur, Phys. Rev. Lett. **59**, 539 (1987).
[4] J. M. Victor and D. Lhuillier, J. Chem. Phys. **92**, 1362 (1990).
[5] M. Bishop and C. J. Saltiel, J. Chem. Phys. **88**, 6594 (1988).
[6] Daniel Lhuillier, J. Phys. (France) **49**, 705 (1988); J. Phys. (France) II **2**, 1411 (1992).
[7] M. E. Fisher, J. Chem. Phys. **44**, 616 (1966).
[8] P. G. de Gennes, *Scaling Concepts in Polymer Physics* (Cornell University Press, Ithaca, NY, 1979).
[9] A. L. Owczarek, T. Prellberg, and R. Brak, Phys. Rev. Lett. **70**, 951 (1993).
[10] J. M. Victor, J-B. Imbert, and D. Lhuillier, J. Chem. Phys. **100**, 5372 (1994).
[11] J. Des Cloizeaux, J. Phys. (Paris) **41**, 223 (1980).
[12] B. Duplantier, J. Phys. A **19**, L1009 (1986).
[13] B. Duplantier, Phys. Rev. B **35**, 5290 (1987).

[14] M. Wittkop, S. Kreitmeier, and D. Göritz, J. Chem. Phys. **104**, 351 (1996).
[15] P. Grassberger, J. Phys. A **26**, 2769 (1993).
[16] F. T. Wall and F. Mandel, J. Chem. Phys. **63**, 4592 (1975); F. Mandel, *ibid.* **70**, 3984 (1979).
[17] J. Carmesin and K. Kremer, Macromolecules **21**, 399 (1988); H. P. Deutsch and K. Binder, J. Chem. Phys. **94**, 2294 (1991).
[18] A. M. Ferrenberg and R. H. Swendsen, Phys. Rev. Lett. **61**, 2635 (1988).
[19] J.-B. Imbert and J. M. Victor, Mol. Simul. **16**, 399 (1996).
[20] N. Madras and A. D. Sokal, J. Stat. Phys. **47**, 573 (1987).
[21] H. Orland, C. Itzykson, and C. de Dominicis, J. Phys. (France) Lett. **46**, 353 (1985).
[22] K. Binder, J. Comput. Phys. **59**, L-55 (1985).
[23] K. Binder, Phys. Rev. Lett. **47**, 693 (1981); K. Binder and D. P. Landau, Phys. Rev. B **30**, 1477 (1984).